~~Inferring horizontal asymmetry~~ Improved estimation of the bulk ice crystal fabric asymmetry from ~~phase-sensitive radar measurements~~ polarimetric phase co-registration

Ole Zeising[1], Tamara Annina Gerber[2], Olaf Eisen[1,3], M. Reza Ershadi[4], Nicolas Stoll[1,3], Ilka Weikusat[1,4], and Angelika Humbert[1,3]

[1]Alfred-Wegener-Institut Helmholtz-Zentrum für Polar- und Meeresforschung, Bremerhaven, Germany
[2]Section for the Physics of Ice, Climate and Earth, The Niels Bohr Institute, University of Copenhagen, Copenhagen, Denmark
[3]Department of Geosciences, University of Bremen, Bremen, Germany
[4]Department of Geosciences, Tübingen University, Tübingen, Germany

Correspondence: Ole Zeising (ole.zeising@awi.de)

Abstract. The bulk crystal orientation in ice influences the flow of glaciers and ice streams. The ice c-axes fabric is most reliably derived from ice cores. Because these are sparse, the spatial and vertical distribution of the fabric in the Greenland and Antarctic ice sheets is largely unknown. In recent years, methods have been developed to determine fabric characteristics from polarimetric radar measurements. The aim of this paper is to present an improved method to infer the horizontal fabric asymmetry by precisely determining the travel-time difference using co-polarised phase-sensitive radar data. We applied this method to six radar measurements from the EastGRIP drill site on Greenland's largest ice stream to give a proof-of-concept by comparing the results with the horizontal asymmetry of the bulk crystal anisotropy derived from the ice core. This comparison shows an almost perfect agreement, which is a large improvement compared to previously used methods. Our approach is particularly useful for determining the vertical profile of the fabric asymmetry in higher resolution and over larger depths than was achievable with previous methods, especially in regions with strong asymmetry.

1   Introduction

The distribution of the crystallographic-axis (c-axis) orientation fabric (henceforth *fabric*) in glaciers and ice sheets is a result of ice deformation history ~~and influences~~ that can influence present-day ice-flow dynamics (Alley, 1988; Faria et al., 2014). Due to the mechanical anisotropy of ice crystals, the bulk viscosity is a directional quantity, spanning several orders of magnitude ~~,~~ depending on the orientation of stresses with respect to the fabric type and orientation (Cuffey and Paterson, 2010).

While some ice-flow models already account for fabric evolution and/or its effect on ice flow (e.g. Thorsteinsson, 2002; Gillet-Chaulet et al., 2006; Seddik et al., 2008; Martín et al., 2009), the validation of these models is ~~obstructed~~ challenged by the lack of in-situ data.

Most reliably, the crystal fabric of ice can be determined from the analysis of ice core thin sections (e.g. Thorsteinsson et al., 1997; Azuma et al., 1999; Wang et al., 2002; Montagnat et al., 2014; Weikusat et al., 2017). Since deep ice cores are sparse in

Greenland and Antarctica, and often restricted to domes with rather undisturbed stratigraphy, little is known about the spatial distribution of crystal fabric anisotropy of ice sheets. It is therefore of great importance to use other methods in order to infer the spatial and vertical distribution of the fabric asymmetry~~.~~, e.g. for improving ice-flow models and determining past flow and deformation.

Ice crystals are uniaxially birefringent (Hargreaves, 1978). This means that ~~crystals also have a dielectric anisotropy in addition to the~~ ice crystals are dielectrically anisotropic due to crystal anisotropy and thus ~~,~~ allow the horizontal fabric asymmetry ~~can also be surveyed using radar measurements~~ to be determined from polarimetric radar surveys (e.g. Fujita et al., 2006; Drews et al., 2012; Leinss et al., 2016; Brisbourne et al., 2019; Jordan et al., 2019, 2020; Young et al., 2021a, b; Ershadi et al., 2022; Jordan et al., 2022; Gerber et al., 2022), with certain limitations (Rathmann et al., 2022). Since polarimetric radar measurements are easier to ~~achieve~~ conduct than ice core analyses, they enable a ~~good~~ greater spatial coverage and thus offer the opportunity to examine the distribution of fabric asymmetry.

For vertically propagating radio waves, the relevant dielectric anisotropy is the difference between the bulk horizontal permittivities (Fujita et al., 2000). One way of inferring the horizontal fabric asymmetry is based on a polarimetric coherence method (Dall, 2010), which refers to the strength of the phase correlation between orthogonal polarisations. This method has recently been applied to polarimetric radar data and compared with the fabric asymmetry from the NEEM ice core in Greenland (Jordan et al., 2019), WAIS divide ice core in West Antarctica (Young et al., 2021a) or the EDML and EDC ice cores in East Antarctica, respectively (Ershadi et al., 2022).

However, this method has some limitations (Leinss et al., 2016). Most importantly, the method can either only be used where the asymmetry of the fabric is weak or otherwise its application is ~~severely~~ limited to shallow depth (Jordan et al., 2022), which we discuss later in detail.

In this study, we infer the horizontal asymmetry of the bulk crystal fabric at the East Greenland Ice Core Project (EastGRIP) drill site from co-polarised phase-sensitive radar measurements by using a new, improved coherence method. This method differs from previously used analysis schemes and has the advantage that the asymmetry can be determined with much higher vertical resolution and, regardless of its strength, up to the onset of the noise level. We present a proof-of-concept by comparing the derived horizontal fabric asymmetry with those from the ice core analysis. A glaciological interpretation of the detected fabric asymmetry regarding the flow dynamics in the region of the EastGRIP drill site is part of a larger study by Gerber et al. (2022) and we refer to their study for ice-dynamical interpretations.

2 Data

In order to investigate ice flow dynamics of Greenland's largest ice stream, the Northeast Greenland Ice Stream (NEGIS), an ice core is being drilled through the $\sim 2668\,\mathrm{m}$ thick ice (Zeising and Humbert, 2021) as part of EastGRIP. In the vicinity of the EastGRIP drill site (75.63 °N, 35.99 °W in 2019), we performed polarimetric measurements with a phase-sensitive radio echo sounder (pRES; Brennan et al. (2014); Nicholls et al. (2015)) in 2019: within the drill trench next to the core location (CL; $\sim 10\,\mathrm{m}$ apart) and at five sites (called $GRID$) within $20 \times 20\,\mathrm{m}^2$ approximately $360\,\mathrm{m}$ from the drill site (Fig. 1). These five sites

are labelled depending on their cardinal direction (N, E, S and W) compared to the centre point (C). The pRES is a ground-based nadir looking Frequency-Modulated Continuous-Wave (FMCW) radar, which allows to determine vertical displacements of reflections within firn and ice from repeated measurements with a high ~~accuracy~~ precision of $\sim 1\,\mathrm{mm}$. While the pRES is mainly operated to derive basal melt rates (e.g. Marsh et al., 2016; Stewart et al., 2019; Zeising et al., 2022), it also can be used to estimate the ice fabric ~~by applying polarimetric pRES measurements (Brisbourne et al., 2019; Jordan et al., 2020; Ershadi et al., 2022)~~ from polarimetric measurements (Brisbourne et al., 2019; Jordan et al., 2020; Young et al., 2021a; Ershadi et al., 2022; Jordan et al., 2022).

A polarimetric pRES measurement consists of several measurements with different antenna orientations. The pRES transmits linearly polarised electromagnetic waves via the transmitting skeleton slot antenna and records the reflected signals in one direction with another antenna. This allows co-polarised measurements to be made in which the two antennas are oriented in the same direction. While in a hh measurement the direction of polarization points to each other, in a vv measurement it is perpendicular to the hh measurement (Fig. 1~~). c~~). Recent studies used quad-polarised acquisitions which additionally include hv and vh measurements, where the polarisation direction of the transmitting and receiving antenna is rotated by $90°$ (e.g. Brisbourne et al., 2019; Young et al., 2021a; Ershadi et al., 2022; Jordan et al., 2022). However, this study focuses on co-polarised measurements.

We aligned the antennas at an arbitrary azimuthal angle of roughly $258°$ (at CL) and $168°$ (at GRID) clockwise to magnetic North ($283°$ and $193°$ true North), respectively. The ice flow direction at EastGRIP is roughly $58°$ magnetic North. We performed multi-polarised measurements by rotating each antenna separately horizontally clockwise in $22.5°$ steps up to $157.5°$. Here, we only considered the co-polarised measurements taken roughly in ice flow direction (hh; $55°$ to magnetic North) and perpendicular to ice flow (vv; $145°$ to magnetic North). During each measurement, the pRES transmitted a sequence of chirps by linearly increasing the transmitted frequency from 200 to $400\,\mathrm{MHz}$ within $1\,\mathrm{s}$ for each chirp. In order to achieve a higher signal-to-noise ratio, the measurement at CL contained 250 chirps and those of the GRID contained 100 chirps per measurement.

3 Methods

3.1 Fabric anisotropy from ice core analysis

~~The fabric data was obtained from continuous 55 cm ice core sections which are basically vertical taken every~~ Every 5–15 m of depth of the ice core a 55 cm long section was analysed for fabric data. Details of the sample preparation, data acquisition and processing are given in Stoll et al. (2021). The grain size weighted orientation of the measured c-~~axis~~ axes can be represented by ~~a second order~~ the second-order orientation tensor. Its normalised eigenvalues

$$\lambda_1 + \lambda_2 + \lambda_3 = 1 \ \text{ and } \ \lambda_1 \le \lambda_2 \le \lambda_3 \tag{1}$$
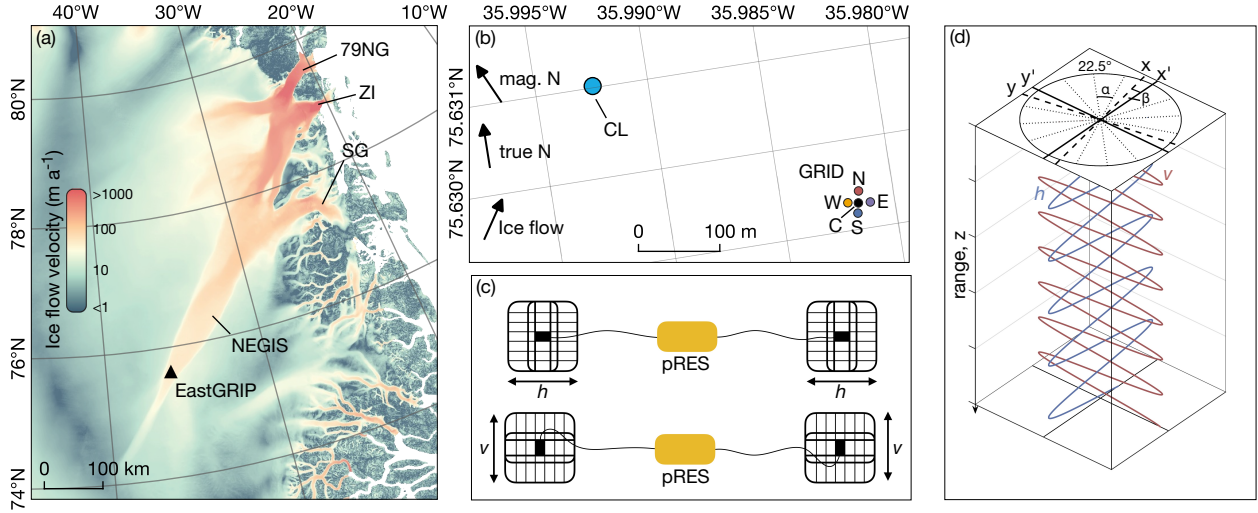
Figure 1. Location and orientation of polarimetric pRES measurements. (a) Surface ice flow velocity of the Greenland Ice Sheet (Joughin et al., 2016, 2018), showing the three major outlet glaciers of the Northeast Greenland Ice Stream (NEGIS): Nioghalvfjerdsbrae (79 N Glacier, 79NG), Zachariæ Isstrøm (ZI) and Storstrømmen Glacier (SG). The location of the EastGRIP drill site is denoted by the black triangle. (b) Location of polarimetric pRES measurements at CL and at GRID. Arrows shown direction of magnetic North, true North and ice flow direction. (c) Sketch of a polarimetric pRES measurement with hh and a vv antenna orientation. (d) Sketch of propagating waves with polarisations in x' (h) and y' (v) direction (solid line) in the x-y coordinate system (dashed line). Dotted lines show the (unused) multi-polarised measurements, separated by $\alpha = 22.5°$. Ice flow is in x direction with an angular offset of β to the hh-measurement in x' direction.

~~correspond to the length~~ quantifies the strength of the three principal ~~axes~~fabric (c-axis) directions. In order to ~~derive~~ determine the fabric asymmetry, we averaged those eigenvalues from all samples of each section and calculated the difference between the eigenvalues ($\lambda_2 - \lambda_1$ and $\lambda_3 - \lambda_1$).

3.2 Horizontal fabric asymmetry from radar measurements

If two electromagnetic waves, whose polarisation in x' and y' are perpendicular to each other, propagate through an anisotropic medium, their ~~propagation velocities~~ depth-averaged propagation velocities $\overline{v}_{x'}$ and $\overline{v}_{y'}$ differ due to the horizontal dielectric anisotropy (Hargreaves, 1978). ~~The resulting difference in two-way travel-time $\Delta t_{x'y'}$ of a backscatter from a reflector at depth z is~~

$$\Delta t_{x'y'}(z) = t_{y'}(z) - t_{x'}(z) = \frac{2\left(\sqrt{\overline{\varepsilon}_{y'}(z)} - \sqrt{\overline{\varepsilon}_{x'}(z)}\right)}{c_0} z,$$

4

$\vdots$

$$\overline{v}_{x'}(z) = \frac{c_0}{\sqrt{\overline{\varepsilon}_{x'}(z)}} = \frac{2z}{t_{x'}(z)}, \tag{2}$$

95

$$\overline{v}_{y'}(z) = \frac{c_0}{\sqrt{\overline{\varepsilon}_{y'}(z)}} = \frac{2z}{t_{y'}(z)} \tag{3}$$

where c_0 is the speed of light in vacuum, $t_{x'}$, $t_{y'}$ are the two-way travel times ~~and~~

$$\overline{\varepsilon}_{x'}(z) \qquad = \frac{c_0^2}{4}\left(\frac{t_{x'}(z)}{z}\right)^2,$$

$$\overline{\varepsilon}_{y'}(z) \quad = \frac{c_0^2}{4}\left(\frac{t_{x'}(z) + \Delta t_{x'y'}(z)}{z}\right)^2$$

~~are the depth-averaged permittivities of the~~ to a reflector at depth z and $\overline{\varepsilon}_{x'}, \overline{\varepsilon}_{y'}$ are the permittivities averaged over the whole

100 depth in the corresponding polarization directions x', y'. The resulting difference in two-way travel-time $\Delta t_{x'y'}$ of a backscatter from a reflector at depth z is

$$\Delta t_{x'y'}(z) = t_{y'}(z) - t_{x'}(z) = \frac{2\left(\sqrt{\overline{\varepsilon}_{y'}(z)} - \sqrt{\overline{\varepsilon}_{x'}(z)}\right)}{c_0} z, \tag{4}$$

and thus the vertical profile of the depth-averaged permittivities are

$$\overline{\varepsilon}_{x'}(z) = \frac{c_0^2}{4}\left(\frac{t_{x'}(z)}{z}\right)^2, \tag{5}$$

105

$$\overline{\varepsilon}_{y'}(z) = \frac{c_0^2}{4}\left(\frac{t_{x'}(z) + \Delta t_{x'y'}(z)}{z}\right)^2. \tag{6}$$

These dielectric permittivities are the average values over the entire depth from the surface to the depth z. In order to ~~obtain~~ calculate the vertical profile of the horizontal dielectric anisotropy $\Delta\varepsilon_{x'y'} = \varepsilon_{y'} - \varepsilon_{x'}$ ~~instead of the depth-average value, the~~ ~~vertical gradient of the travel-times has~~ , the local change in two-way travel time $\delta t_{x'}$, $\delta t_{y'}$ for a given infinitesimal depth window δz, needs to be taken into account:

110

$$\varepsilon_{x'}(z) = \frac{c_0^2}{4}\left(\frac{dt_{x'}(z)}{dz}\frac{\delta t_{x'}(z)}{\delta z}\right)^2, \tag{7}$$

$$\varepsilon_{y'}(z) = \frac{c_0^2}{4}\left(\frac{d(t_{x'}(z) + \Delta t_{x'y'}(z))}{dz}\frac{\delta(t_{x'}(z) + \Delta t_{x'y'}(z))}{\delta z}\right)^2. \tag{8}$$

~~According to Fujita et al. (2006) and Jordan et al. (2019), the~~ If it is assumed that the ice crystals are an effective medium at ice penetrating frequencies, the bulk horizontal dielectric anisotropy for the two polarisations in x' and y' direction, $\Delta\varepsilon_{x'y'}$, is a function of the horizontal fabric asymmetry $\Delta\lambda_{x'y'} = \lambda_{y'} - \lambda_{x'}$ and of the dielectric anisotropy of an ice crystal $\Delta\varepsilon'$:

115

$$\Delta\varepsilon_{x'y'}(z) = \varepsilon_{y'}(z) - \varepsilon_{x'}(z) = \Delta\varepsilon'(\lambda_{y'}(z) - \lambda_{x'}(z)) = \Delta\varepsilon'\Delta\lambda_{x'y'}(z). \tag{9}$$

(Fujita et al., 2006; Jordan et al., 2019). This assumes that the wavelength is much longer than the average grain size, which is the case for the frequency range from 200 to 400 MHz and the corresponding wavelengths from 0.42 to 0.84 m. Matsuoka et al. (1997) found $\Delta\varepsilon' = 0.034$ for ice-penetrating radar frequencies. Finally, the horizontal fabric asymmetry $\Delta\lambda_{x'y'}$ at depth z is given by

$$\Delta\lambda_{x'y'}(z) = \lambda_{y'}(z) - \lambda_{x'}(z) = \frac{\Delta\varepsilon_{x'y'}(z)}{\Delta\varepsilon'}. \tag{10}$$

Thus, the bulk dielectric anisotropy $\Delta\varepsilon_{x'y'}$, and based on this, the horizontal fabric asymmetry $\Delta\lambda_{x'y'}$ can be determined from the difference in the two-way travel time $\Delta t_{x'y'}$. The vertical resolution of $\Delta\lambda_{x'y'}$ depends on the precise determination of $\Delta t_{x'y'}$, which used to be a problem for previous radar systems that did not have the required resolution in the time domain. This is the main ~~difference to and~~ advantage of the in-depth analysis of the phase which is why polarimetric pRES measurements offer the chance to investigate the horizontal fabric asymmetry in the ice.

3.3 Phase-sensitive radar data analysis

For data processing, we followed Brennan et al. (2014) and Stewart et al. (2019) in order to get the complex valued signals $\boldsymbol{s}_{hh}$ and $\boldsymbol{s}_{vv}$ (subscripts indicate the transmitted and received polarisation) as a function of two-way travel time with the amplitude $|\boldsymbol{s}_{hh}|$ and its phase. We convert $\boldsymbol{s}$ from time t to depth z domain by using dielectric permittivities derived from dielectric profiling (DEP) of the EastGRIP ice core by Mojtabavi et al. (2020).

The method we apply to compute the travel-time difference $\Delta t_{x'y'}$ is based on a cross-correlation of the co-polarised measurements. The same method is widely used to estimate vertical displacements for strain analysis from repeated pRES measurements as shown by e.g. Jenkins et al. (2006), Gillet-Chaulet et al. (2011), Stewart et al. (2019) and Zeising and Humbert (2021). We divided $\boldsymbol{s}_{hh}$ into segments of 12 m depth overlapping by 9 m and calculated for each the complex coherence

$$\boldsymbol{c}_{hhvv}(z,l) = \frac{\sum_{j=z_n}^{z_n+N} \boldsymbol{s}_{hh}(j)\boldsymbol{s}_{vv}^*(j+l)}{\sqrt{\sum_{j=z_n}^{z_n+N} |\boldsymbol{s}_{hh}(j)|^2}\sqrt{\sum_{j=z_n}^{z_n+N} |\boldsymbol{s}_{vv}(j+l)|^2}} \frac{\sum_{j=i_n}^{i_n+N} \boldsymbol{s}_{hh}(j)\boldsymbol{s}_{vv}^*(j+l)}{\sqrt{\sum_{j=i_n}^{i_n+N} |\boldsymbol{s}_{hh}(j)|^2}\sqrt{\sum_{j=i_n}^{i_n+N} |\boldsymbol{s}_{vv}(j+l)|^2}}, \tag{11}$$

where ~~z_n~~ i_n is the lower ~~range bin~~ time-bin index of the segment, N the number of bins in the segment, l the range-bin offset (lag) and * indicates the complex conjugate (Stewart et al., 2019). While the magnitude of the complex coherence $|\boldsymbol{c}_{hhvv}|$ is the correlation between $\boldsymbol{s}_{hh}$ and $\boldsymbol{s}_{vv}$, the argument is the coherence phase $\phi_{hhvv} = \arg(\boldsymbol{c}_{hhvv})$ (Jordan et al., 2019).

Our *polarimetric cross-correlation* approach differs from the *coherence* method from Dall (2010) that was used by Jordan et al. (2019, 2020, 2022), Young et al. (2021a) and Ershadi et al. (2022). In their applications, the range-bin offset was set to zero ($l = 0$). Thus, these studies interpreted the $hhvv$ coherence phase gradient of the same two-way travel-time. In ~~our~~ this study, we are analysing the travel-time difference of the same reflector that we determine from a cross-correlation ~~method, we shift~~ approach. We co-register the phase of $\boldsymbol{s}_{hh}$ and $\boldsymbol{s}_{vv}$ for every segment by shifting $\boldsymbol{s}_{vv}$ by a number of integer bin offsets l (see eq. 11). ~~This enables the possibility to analyse the travel-time difference of the same reflector.~~ We identified the correct l of each segment by following the minimum phase difference from the surface downwards, indicated by high correlation values (Fig. 2b,c).

6
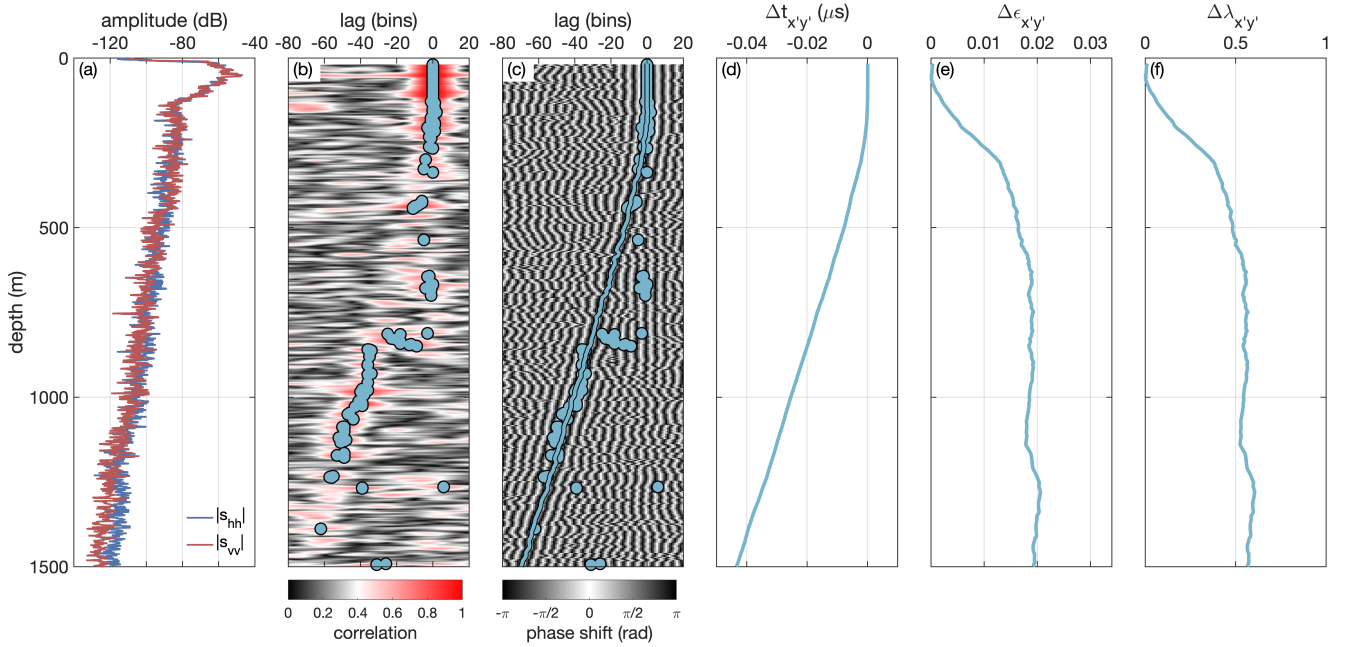
Figure 2. Analysis of the horizontal fabric asymmetry from polarimetric pRES measurements at the location CL (Fig. 1) next to the EastGRIP ice core. (a) Magnitude profiles of s_{hh} (blue line) and s_{vv} (red line) as a function of depth. (b) Cross-correlation $|c_{hhvv}|$ of s_{hh} and s_{vv} as a function of lag and depth. Blue dots mark the lag of best correlation for each segment exceeding a correlation of 0.65. (c) Coherence phase shift ϕ_{hhvv} as a function of lag and depth. The blue dots are the same as in (b). The blue line marks the tracked minimum phase shift. (d) Difference in two-way travel time between both measurements at the same depth after smoothing with a $100\,\text{m}$ moving average filter. (e) Difference in horizontal dielectric anisotropy $\Delta\varepsilon_{x'y'}$. (f) Difference in horizontal eigenvalues $\Delta\lambda_{x'y'}$.

Next, we ~~derived~~ compute the travel-time difference $\Delta t_{x'y'}$ (Fig. 2d) ~~from the sum of the range-bin offset~~ for each segment based on the selected lag l and the corresponding ~~phase shift~~ coherent phase ϕ_{hhvv} (see Brennan et al., 2014):

$$\Delta t_{x'y'}(z) = \frac{l(z)}{Bp} + \frac{\phi_{hhvv}(z)}{2\pi f_c} \frac{\phi_{hhvv}(l,z)}{2\pi f_c}. \tag{12}$$

150 ~~where~~ The first term on the right side is the coarse time-bin offset with $1/Bp$ being the time-bin spacing ($B = 200\,\text{MHz}$ is the bandwidth and $p = 8$ is a 'padding factor' that reduces the range-bin spacing, ~~$B = 200\,\text{MHz}$ is the bandwidth and $f_c = 300\,\text{MHz}$ the~~). The second term is the fine offset derived from the coherent phase of the centre frequency of ~~the pRES measurement (see Brennan et al., 2014)~~ $f_c = 300\,\text{MHz}$.

Since the travel-time difference is cumulative, we calculated the mean vertical ~~gradient~~ change of the two-way travel times, ~~$dt_{x'}/dz$ and $d(t_{x'} + \Delta t_{x'y'})/dz$~~ $\delta t_{x'}/\delta z$ and $\delta(t_{x'} + \Delta t_{x'y'})/\delta z$, from a $200\,\text{m}$ moving window after smoothing $\Delta t_{x'y'}$ with a
155 $100\,\text{m}$ moving average filter. ~~Below~~ Between the surface and $100\,\text{m}$ depth, we ~~adopted~~ changed the method to use a smaller, adaptive moving window that increases with depth. Finally, we compute the dielectric anisotropy $\Delta\varepsilon_{x'y'}$ from Eqs. 8 and 9 (Fig. 2e) and the horizontal fabric asymmetry $\Delta\lambda_{x'y'}$ from Eq. 10 (Fig. 2f).

7

4 Results

The horizontal fabric asymmetry from the polarimetric cross-correlation analysis at all measurement locations show the same vertical distribution with only minor differences (Fig. 3a). They indicate a rapid increase of $\Delta\lambda_{x'y'}$ from 0.06 to 0.4 within the first 12% of the ice thickness between 125 and 320 m depth~~,~~. This is followed by a minor increase to 0.55, reached at a depth of 550 m (20% of the ice thickness). Between this depth and 1400 m, the horizontal anisotropy remains at high level and varies between 0.52 and 0.62. Below the depth of ~~1400 m~~1400 m, a low signal-to-noise ratio prevented the analysis of the horizontal fabric asymmetry. This depth corresponds to 52% of the ice thickness.

In order to demonstrate the improvement over the previous coherence method, we also applied the method from Young et al. (2021a), which is based on the work of Jordan et al. (2019, 2020). The results show the same vertical profile only between 100 and 260 m. Below, the horizontal asymmetry drops to near zero and differs strongly from the result of the new cross-correlation method.

The pRES-derived vertical distribution matches the distribution of the difference of the weighted horizontal eigenvalues from the EastGRIP ice core analysis nearly perfectly (Fig. 3b).

While the differences of the first two eigenvalues ($\lambda_2 - \lambda_1$) show the same rapid increase between 125 and 250 m depth, below, it is $\lambda_3 - \lambda_1$ that is of the same size than the pRES-derived values. This indicates that one of the horizontal eigenvalues becomes the largest value (λ_3 by definition) at a depth of 250 m and thus λ_3 switches from the vertical to one horizontal axis. However, since $\Delta\lambda_{x'y'}$ exceeds 0.5, it is obvious that a horizontal eigenvalue is the largest since the $\lambda_2 - \lambda_1$ is always ≤ 0.5.

~~The mean deviation of the horizontal fabric asymmetry derived from polarimetric pRES measurements and the difference of the weighted horizontal eigenvalues from the ice core analysis ($\lambda_2 - \lambda_1$ between 120 and 250 m and $\lambda_3 - \lambda_1$ between 250 and 1400 m) is only 0.03 and thus of the same size than the uncertainty of the ice core analysis. However, the mean deviation to the difference of the unweighted horizontal eigenvalue is higher, which is a result compatible to analyses of seismic waves by Kerch et al. (2018).~~

5 Discussion

Our polarimetric cross-correlation method allows to resolve the travel-time difference of the co-polarised waves with sub-nanoseconds resolution. On this basis, the vertical ~~distribution~~ profile of the horizontal dielectric anisotropy as well as the bulk crystal fabric asymmetry can be determined. Despite the high range resolution, the scatter of $\Delta t_{x'y'}$ caused by the uncertainty prevented a ~~small-scale~~ determination of the small-scale gradient of the travel-time difference. Thus, the derived horizontal anisotropy only represents a coarse distribution. The horizontal fabric asymmetry derived from the polarimetric cross-correlation of the pRES measurements and the difference of the weighted horizontal eigenvalues from the ice core analysis ($\lambda_2 - \lambda_1$ between 120 and 250 m and $\lambda_3 - \lambda_1$ between 250 and 1400 m) show almost perfect agreement with a root-mean-square difference of the result of both methods of only 0.03. This value corresponds to the uncertainty of the ice core analysis and thus represents the lowest possible value in the difference. However, the root-mean-square value of the
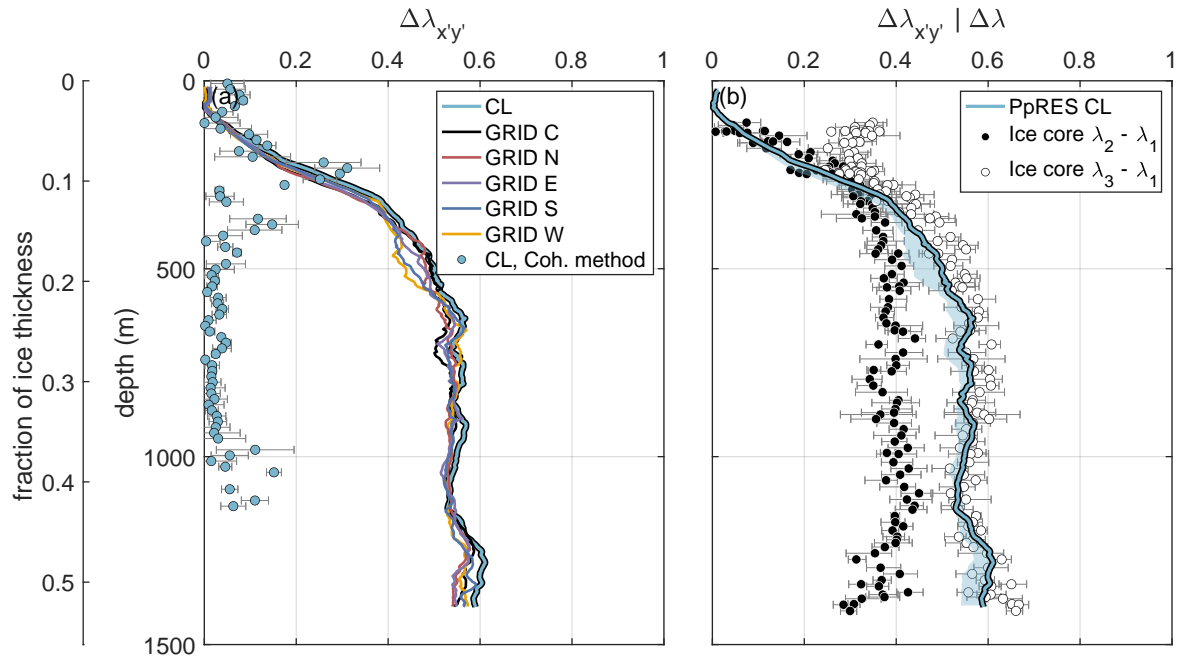
Figure 3. ~~Horizontal~~ Comparison of horizontal fabric asymmetry $\Delta\lambda$ ~~derived~~ determined from ~~polarimetric~~ different measurements and analysing methods. (a) Fabric asymmetry determined from cross-correlation analysis (lines) of pRES measurements at CL (light blue line) ~~, compared with (a) analysed polarimetric pRES measurements~~ and at the $20 \times 20\,\mathrm{m}$ GRID outside drill site as well as from the previous coherence method (Young et al., 2021a) at CL (~~all analysed with our new approach~~light blue dots)~~and~~. (b) ~~fabric~~ Fabric asymmetry ~~derived~~ determined from ~~the~~ cross-correlation analysis (lines) of pRES measurements at CL (light blue line) and from weighted horizontal eigenvalues from EastGRIP ice core (black and white dots). The blue shaded area in (b) marks the range of the polarimetric pRES-derived asymmetry from the measurements in the GRID and at CL.

difference of the unweighted horizontal eigenvalue is 0.06 and thus higher, which is a result compatible to analyses of seismic waves by Kerch et al. (2018).

The determination of the horizontal asymmetry is not possible for every azimuthal angle. The azimuth angle of the antenna has to match the alignment of the orientation of the ice fabric principal axes sufficiently. If the direction of polariza-

195 tion is rotated $45°$ to the alignment of the principal axes, no anisotropy can be determined, as the propagation velocity is the same in x' and y' direction. The polarimetric pRES measurements at EastGRIP show that with an azimuthal rotation of the antennas with $22.5°$ increments up to $67.5°$, a determination is possible in two of the four orientations and that the derived horizontal anisotropy is identical in both cases. ~~In that sense, polarimetric pRES measurements allow to determine the fabric orientation within the rotation intervals (in this case 22.5°). However, Ershadi et al. (2022) presented a method~~

200 ~~which allows to perform measurements from only~~ However, a clear advantage of quad-polarised measurements is that they allow to reconstruct co-polarised data at a high angular resolution and additionally the determination of the fabric orientation

(e.g. Brisbourne et al., 2019; Young et al., 2021a; Ershadi et al., 2022; Jordan et al., 2022). The presented cross-correlation method can also be applied to these reconstructed co-polarised data. Since only four measurements (hh, vv, hv and vh) at one azimuthal angle ~~and to calculate the maximum horizontal asymmetry based on synthesizing the other angles~~ are necessary to perform a quad-polarised acquisition, but eight for co-polarised measurement (hh and vv) at four different azimuthal angles (0°, 22.5°, 45° and 67.5°), quad-polarised measurements should be preferred in the future.

~~Due to the ambiguities caused by phase wrapping, the previous methods which are based on the coherence phase gradient were limited to the derivation of~~

The previously used coherence method estimates the fabric asymmetry by determining the phase ~~shifts of a maximum of half a wavelength. This limits the depth to which fabric asymmetry can be determined: The more pronounced the asymmetry, the greater the difference in propagation velocity and thus the half-wavelength limit is reached earlier~~ gradient of the polarimetric phase difference. This is also possible for high coherence persisting over a few phase cycles (e.g., Young et al., 2021a). However, in case of a strongly developed fabric asymmetry and thus a rapid phase-cycling, the coherence is reduced over depth because the segments that are correlated do not completely overlap and therefore contain different scatterers (Leinss et al., 2016). At ice divides or domes with very little asymmetry, such as at NEEM (Jordan et al., 2019), WAIS divide (Young et al., 2021a) or EDC (Ershadi et al., 2022), the fabric asymmetry could successfully be determined using ~~the~~ previous coherence method up to the onset of noise. However, in fast moving areas like the Rutford Ice Stream, Antarctica (Jordan et al., 2022) or NEGIS, Greenland (this study) ~~the previous method is limited~~ rapid phase-cycling limits the application of the previous coherence method to a few hundred meters below the surface. ~~At EastGRIP, the phase shift at $l = 0$ exceeds half a wavelength at a depth of 250 m, which significantly limits the application of the previous coherence method in contrast to our approach. Below 250 m, the correlation drops at $l = 0$ (Fig. 2b), since the correlated reflections occurred from different reflectors that are more than half a wavelength apart. This may also be the reason for the low coherence magnitude in the analysis results from Jordan et al. (2022), which is why the evaluation of the pRES measurements at the Rutford Ice Stream, Antarctica was only possible down to a maximum depth of 300 m. With our~~ With the improved polarimetric cross-correlation method, we overcome this limitation through co-registration, which allows to determine even strong horizontal fabric asymmetries to a much greater depth. Noise limits the evaluation of fabric asymmetry for deeper layers. At the EastGRIP drill site, this limit is about half the ice thickness of the ice with current systems. Determining the fabric for deeper layers from radar measurements, eventually over the whole ice sheet thickness, requires further reduction of the signal-to-noise ratio in more powerful phase-sensitive radar system that can perform co- or quad-polarized measurements. The applicability of the polarimetric cross-correlation method ~~, which is based on phase unwrapping, this limitation can be overcome and phase shifts greater than half a wavelength can be evaluated. This allows the determination of even strong horizontal fabric asymmetries to a much greater depth.~~ needs first to be demonstrated for such radar systems.

Ershadi et al. (2022) presented a method to estimate horizontal ice fabric anisotropy based on a non-linear inverse approach ~~and synthesized polarimetric radar data~~ by using the coherence phase gradient and power anomaly. Here we tried to use this method on our data to compare the two methods directly. However, the ice fabric orientation in this area rotates several times at different depths of the ice column, which ~~is the main limitation~~ prevents the application of the previous method using the

inverse approach. Therefore, the attempt for direct comparison ~~has failed which is another proof that our method has improved the previous method and goes beyond its~~ was unsuccessful and is another reason why we regard our method as an improvement which goes beyond previous limits.

6 Conclusions

We presented a new method to infer the vertical profile of the horizontal fabric asymmetry from polarimetric phase-sensitive radar measurements. Our approach is based on a cross-correlation of co-polarised measurements to derive precisely travel-time differences caused by dielectric anisotropy. In contrast to previous methods, this polarimetric cross-correlation approach allows to analyse even strong horizontal fabric asymmetries ~~to~~ at a much greater depth.

The remarkable agreement between the vertical profile of the horizontal fabric asymmetry obtained by our analyses of multiple polarimetric pRES measurements and the fabric measured in the EastGRIP ice core demonstrates the robustness and precision of our method.

In the future, the applicability of our polarimetric cross-correlation method to other radar systems should be tested, in particular to polarimetric airborne radar measurements. If successful, this would increase the spatial coverage of mapped crystal fabric and its variability than would be possible with pointwise polarimetric pRES measurements. Furthermore, it might allow the estimation of the fabric to greater depth. Such an application ~~would~~, which would yield the variation of the horizontal anisotropy along flow lines or across regions of fast flow, like ice streams, would significantly improve the understanding of the link between the stress state and crystal fabric evolution ~~and allow~~. This would allow us to decrease uncertainties of rheology, and thus improve estimates for response times of dynamically active glacial systems ~~, like ice streams,~~ to external perturbations~~.~~, e.g. from changing ocean conditions of tidewater glaciers.

References

275   Alley, R. B.: Fabrics in Polar Ice Sheets: Development and Prediction, Science, 240, 493–495, https://doi.org/10.1126/science.240.4851.493, 1988.

Azuma, N., Wang, Y., Mori, K., Narita, H., Hondoh, T., Shoji, H., and Watanabe, O.: Textures and fabrics in the Dome F (Antarctica) ice core, Annals of Glaciology, 29, 163–168, https://doi.org/10.3189/172756499781821148, 1999.

Brennan, P. V., Lok, L. B., Nicholls, K., and Corr, H.: Phase-sensitive FMCW radar system for high-precision Antarctic ice shelf profile
280   monitoring, IET Radar, Sonar & Navigation, 8, 776–786, https://doi.org/10.1049/iet-rsn.2013.0053, 2014.

Brisbourne, A. M., Martín, C., Smith, A. M., Baird, A. F., Kendall, J. M., and Kingslake, J.: Constraining Recent Ice Flow History at Korff Ice Rise, West Antarctica, Using Radar and Seismic Measurements of Ice Fabric, Journal of Geophysical Research: Earth Surface, 124, 175–194, https://doi.org/10.1029/2018JF004776, 2019.

Cuffey, K. M. and Paterson, W. S. B.: The Physics of Glaciers - 4th ed., Elsevier, 2010.

285   Dall, J.: Ice sheet anisotropy measured with polarimetric ice sounding radar, in: 2010 IEEE International Geoscience and Remote Sensing Symposium, pp. 2507–2510, https://doi.org/10.1109/IGARSS.2010.5653528, 2010.

Drews, R., Eisen, O., Steinhage, D., Weikusat, I., Kipfstuhl, S., and Wilhelms, F.: Potential mechanisms for anisotropy in ice-penetrating radar data, Journal of Glaciology, 58, 613–624, https://doi.org/10.3189/2012JoG11J114, 2012.

Ershadi, M. R., Drews, R., Martín, C., Eisen, O., Ritz, C., Corr, H., Christmann, J., Zeising, O., Humbert, A., and Mulvaney, R.: Po-
290   larimetric radar reveals the spatial distribution of ice fabric at domes and divides in East Antarctica, The Cryosphere, 16, 1719–1739, https://doi.org/10.5194/tc-16-1719-2022, 2022.

Faria, S. H., Weikusat, I., and Azuma, N.: The microstructure of polar ice. Part II: State of the art, Journal of Structural Geology, 61, 21–49, https://doi.org/10.1016/j.jsg.2013.11.003, 2014.

Fujita, S., Matsuoka, T., Ishida, T., Matsuoka, K., and Mae, S.: A summary of the complex dielectric permittivity of ice in the megahertz
295   range and its applications for radar sounding of polar ice sheets, in: Physics of ice core records, pp. 185–212, Hokkaido University Press, 2000.

Fujita, S., Maeno, H., and Matsuoka, K.: Radio-wave depolarization and scattering within ice sheets: a matrix-based model to link radar and ice-core measurements and its application, Journal of Glaciology, 52, 407–424, https://doi.org/10.3189/172756506781828548, 2006.

Gerber, T., Lilien, D., Rathmann, N., Franke, S., Young, T. J., Valero-Delgado, F., Ershadi, R., Drews, R., Zeising, O., Humbert, A., Stoll, N.,
300   Weikusat, I., Grinsted, A., Hvidberg, C., Jansen, D., Miller, H., Helm, V., Steinhage, D., O'Neill, C., Gogineni, P., Paden, J., Dahl-Jensen, D., and Eisen, O.: Crystal fabric anisotropy causes directional hardening of the Northeast Greenland Ice Stream, Preprint (Version 1), available at Research Square, https://doi.org/10.21203/rs.3.rs-1812870/v1, 2022.

Gillet-Chaulet, F., Gagliardini, O., Meyssonnier, J., Zwinger, T., and Ruokolainen, J.: Flow-induced anisotropy in polar ice and related ice-sheet flow modelling, Journal of Non-Newtonian Fluid Mechanics, 134, 33–43, https://doi.org/10.1016/j.jnnfm.2005.11.005, 2nd Annual
305   European Rheology Conference, 2006.

Gillet-Chaulet, F., Hindmarsh, R. C. A., Corr, H. F. J., King, E. C., and Jenkins, A.: In-situ quantification of ice rheology and direct measurement of the Raymond Effect at Summit, Greenland using a phase-sensitive radar, Geophysical Research Letters, 38, https://doi.org/10.1029/2011GL049843, 2011.

Hargreaves, N. D.: The Radio-Frequency Birefringence of Polar Ice, Journal of Glaciology, 21, 301–313,
310   https://doi.org/10.3189/S0022143000033499, 1978.

13

Jenkins, A., Corr, H. F., Nicholls, K. W., Stewart, C. L., and Doake, C. S.: Interactions between ice and ocean observed with phase-sensitive radar near an Antarctic ice-shelf grounding line, Journal of Glaciology, 52, 325–346, https://doi.org/10.3189/172756506781828502, 2006.

Jordan, T. M., Schroeder, D. M., Castelletti, D., Li, J., and Dall, J.: A Polarimetric Coherence Method to Determine Ice Crystal Orientation Fabric From Radar Sounding: Application to the NEEM Ice Core Region, IEEE Transactions on Geoscience and Remote Sensing, 57, 8641–8657, https://doi.org/10.1109/TGRS.2019.2921980, 2019.

Jordan, T. M., Schroeder, D. M., Elsworth, C. W., and Siegfried, M. R.: Estimation of ice fabric within Whillans Ice Stream using polarimetric phase-sensitive radar sounding, 61, 74–83, https://doi.org/10.1017/aog.2020.6, 2020.

Jordan, T. M., Martín, C., Brisbourne, A. M., Schroeder, D. M., and Smith, A. M.: Radar Characterization of Ice Crystal Orientation Fabric and Anisotropic Viscosity Within an Antarctic Ice Stream, Journal of Geophysical Research: Earth Surface, 127, e2022JF006 673, https://doi.org/10.1029/2022JF006673, 2022.

Joughin, I., Smith, B., Howat, I., and Scambos, T.: MEaSUREs Multi-year Greenland Ice Sheet Velocity Mosaic, Version 1. Boulder, Colorado USA. NASA National Snow and Ice Data Center Distributed Active Archive Center [data set], https://doi.org/10.5067/QUA5Q9SVMSJG., 2016.

Joughin, I., Smith, B. E., and Howat, I. M.: A complete map of Greenland ice velocity derived from satellite data collected over 20 years, Journal of Glaciology, 64, 1–11, https://doi.org/10.1017/jog.2017.73, 2018.

Kerch, J., Diez, A., Weikusat, I., and Eisen, O.: Deriving micro- to macro-scale seismic velocities from ice-core c axis orientations, The Cryosphere, 12, 1715–1734, https://doi.org/10.5194/tc-12-1715-2018, 2018.

Leinss, S., Löwe, H., Proksch, M., Lemmetyinen, J., Wiesmann, A., and Hajnsek, I.: Anisotropy of seasonal snow measured by polarimetric phase differences in radar time series, The Cryosphere, 10, 1771–1797, https://doi.org/10.5194/tc-10-1771-2016, 2016.

Marsh, O. J., Fricker, H. A., Siegfried, M. R., Christianson, K., Nicholls, K. W., Corr, H. F., and Catania, G.: High basal melting forming a channel at the grounding line of Ross Ice Shelf, Antarctica, Geophysical Research Letters, 43, 250–255, https://doi.org/10.1002/2015GL066612, 2016.

Martín, C., Gudmundsson, G. H., Pritchard, H. D., and Gagliardini, O.: On the effects of anisotropic rheology on ice flow, internal structure, and the age-depth relationship at ice divides, Journal of Geophysical Research: Earth Surface, 114, https://doi.org/10.1029/2008JF001204, 2009.

Matsuoka, T., Fujita, S., Morishima, S., and Mae, S.: Precise measurement of dielectric anisotropy in ice Ih at 39 GHz, Journal of Applied Physics, 81, 2344–2348, https://doi.org/10.1063/1.364238, 1997.

Mojtabavi, S., Wilhelms, F., Cook, E., Davies, S. M., Sinnl, G., Skov Jensen, M., Dahl-Jensen, D., Svensson, A., Vinther, B. M., Kipfstuhl, S., Jones, G., Karlsson, N. B., Faria, S. H., Gkinis, V., Kjær, H. A., Erhardt, T., Berben, S. M. P., Nisancioglu, K. H., Koldtoft, I., and Rasmussen, S. O.: A first chronology for the East Greenland Ice-core Project (EGRIP) over the Holocene and last glacial termination, Climate of the Past, 16, 2359–2380, https://doi.org/10.5194/cp-16-2359-2020, 2020.

Montagnat, M., Azuma, N., Dahl-Jensen, D., Eichler, J., Fujita, S., Gillet-Chaulet, F., Kipfstuhl, S., Samyn, D., Svensson, A., and Weikusat, I.: Fabric along the NEEM ice core, Greenland, and its comparison with GRIP and NGRIP ice cores, The Cryosphere, 8, 1129–1138, https://doi.org/10.5194/tc-8-1129-2014, 2014.

Nicholls, K. W., Corr, H. F., Stewart, C. L., Lok, L. B., Brennan, P. V., and Vaughan, D. G.: A ground-based radar for measuring vertical strain rates and time-varying basal melt rates in ice sheets and shelves, Journal of Glaciology, 61, 1079–1087, https://doi.org/10.3189/2015JoG15J073, 2015.

Rathmann, N. M., Lilien, D. A., Grinsted, A., Gerber, T. A., Young, T. J., and Dahl-Jensen, D.: On the Limitations of Using Polarimetric Radar Sounding to Infer the Crystal Orientation Fabric of Ice Masses, Geophysical Research Letters, 49, e2021GL096 244,

350   https://doi.org/10.1029/2021GL096244, 2022.

Seddik, H., Greve, R., Placidi, L., Hamann, I., and Gagliardini, O.: Application of a continuum-mechanical model for the flow of anisotropic polar ice to the EDML core, Antarctica, Journal of Glaciology, 54, 631–642, https://doi.org/10.3189/002214308786570755, 2008.

Stewart, C. L., Christoffersen, P., Nicholls, K. W., Williams, M. J., and Dowdeswell, J. A.: Basal melting of Ross Ice Shelf from solar heat absorption in an ice-front polynya, Nature Geoscience, 12, 435–440, https://doi.org/10.1038/s41561-019-0356-0, 2019.

355   Stoll, N., Eichler, J., Hörhold, M., Erhardt, T., Jensen, C., and Weikusat, I.: Microstructure, micro-inclusions, and mineralogy along the EGRIP ice core – Part 1: Localisation of inclusions and deformation patterns, The Cryosphere, 15, 5717–5737, https://doi.org/10.5194/tc-15-5717-2021, 2021.

Thorsteinsson, T.: Fabric development with nearest-neighbor interaction and dynamic recrystallization, Journal of Geophysical Research: Solid Earth, 107, ECV 3–1–ECV 3–13, https://doi.org/10.1029/2001JB000244, 2002.

360   Thorsteinsson, T., Kipfstuhl, J., and Miller, H.: Textures and fabrics in the GRIP ice core, Journal of Geophysical Research: Oceans, 102, 26 583–26 599, https://doi.org/10.1029/97JC00161, 1997.

Wang, Y., Thorsteinsson, T., Kipfstuhl, J., Miller, H., Dahl-Jensen, D., and Shoji, H.: A vertical girdle fabric in the NorthGRIP deep ice core, North Greenland, Annals of Glaciology, 35, 515–520, https://doi.org/10.3189/172756402781817301, 2002.

Weikusat, I., Jansen, D., Binder, T., Eichler, J., Faria, S. H., Wilhelms, F., Kipfstuhl, S., Sheldon, S., Miller, H., Dahl-Jensen, D., et al.:

365   Physical analysis of an Antarctic ice core—towards an integration of micro-and macrodynamics of polar ice, Philosophical Transactions of the Royal Society A: Mathematical, Physical and Engineering Sciences, 375, 20150 347, https://doi.org/10.1098/rsta.2015.0347, 2017.

Young, T. J. and Dawson, E. J.: Quad-polarimetric ApRES measurements along a 6 km-long transect at the WAIS Divide, December 2019 (Version 1.0), NERC EDS UK Polar Data Centre [data set], https://doi.org/10.5285/BA1CAF7A-D4E0-4671-972A- E567A25CCD2C, 2021.

370   Young, T. J., Martín, C., Christoffersen, P., Schroeder, D. M., Tulaczyk, S. M., and Dawson, E. J.: Rapid and accurate polarimetric radar measurements of ice crystal fabric orientation at the Western Antarctic Ice Sheet (WAIS) Divide ice core site, The Cryosphere, 15, 4117–4133, https://doi.org/10.5194/tc-15-4117-2021, 2021a.

Young, T. J., Schroeder, D. M., Jordan, T. M., Christoffersen, P., Tulaczyk, S. M., Culberg, R., and Bienert, N. L.: Inferring Ice Fabric From Birefringence Loss in Airborne Radargrams: Application to the Eastern Shear Margin of Thwaites Glacier, West Antarctica, Journal of

375   Geophysical Research: Earth Surface, 126, e2020JF006 023, https://doi.org/10.1029/2020JF006023, 2021b.

Zeising, O. and Humbert, A.: Indication of high basal melting at the EastGRIP drill site on the Northeast Greenland Ice Stream, The Cryosphere, 15, 3119–3128, https://doi.org/10.5194/tc-15-3119-2021, 2021.

Zeising, O. and Humbert, A.: Polarimetric phase-sensitive radar measurements at EastGRIP drill site, Alfred Wegener Institute, Helmholtz Centre for Polar and Marine Research, Bremerhaven, PANGAEA [data set], https://doi.org/10.1594/PANGAEA.951267, 2022.

380   Zeising, O., Steinhage, D., Nicholls, K. W., Corr, H. F. J., Stewart, C. L., and Humbert, A.: Basal melt of the southern Filchner Ice Shelf, Antarctica, The Cryosphere, 16, 1469–1482, https://doi.org/10.5194/tc-16-1469-2022, 2022.